



Carboxylated alginate hydrogel beads for methylene blue removal: formulation, kinetic and isothermal studies

Mohamed Samir Mohy Eldin^{a,*}, Emad Ali Soliman^a, Ahmed Abdel Fattah Elzatahry^a, Mohamed Ramadan Elaassar^{a,#}, Bassant Yossri Eweida^a, Marwa Farouk Elkady^{b,c}, Aref Mohamed Abdel Rahman^d, Mohamed Elsayed Yossef^e

^aPolymer Materials Research Department, Advanced Technology and New Materials Research Institute, City of Scientific Research and Technological Applications (SRTA-City), New Borg El-Arab City, 21934, Alexandria, Egypt, Tel./Fax: +203 4593 414; emails: mohyeldinmohamed@gmail.com (M.S. Mohy Eldin), emadsoliman@gmail.com (E.A. Soliman), elzatahry@gmail.com (A.A. Elzatahry), mohamed.elaassar@gmail.com (M.R. Elaassar), Basant177@yahoo.com (B.Y. Eweida)

^bChemical and Petrochemical Engineering Department, Egypt-Japan University of Science and Technology (E-JUST), New Borg El-Arab City, Alexandria 21934, Egypt, email: marwa.f.elkady@gmail.com

^cFabrication Technology Department, Advanced Technology and New Materials Research Institute, City of Scientific Research and Technological Applications (SRTA-City), New Borg El-Arab City, 21934, Alexandria, Egypt

^dNano and Composite Materials Research Department, Advanced Technology and New Materials Research Institute, City of Scientific Research and Technological Applications (SRTA-City), New Borg El-Arab City, 21934, Alexandria, Egypt, email: drareff@gmail.com

^eComputer Based Engineering Applications, Informatic Research Institute, City of Scientific Research and Technological Applications (SRTA-City), New Borg El-Arab City, 21934, Alexandria, Egypt, email: elsayed168@gmail.com

Received 22 December 2018; Accepted 28 June 2019

ABSTRACT

In this study, carboxylated alginate beads for methylene blue (MB) removal have developed, and the formulation conditions such as alginate concentration, calcium chloride concentration, cross-linking temperature, and beads size have been studied. The influence of various parameters such as initial MB concentration, contact time and adsorbent dosage on MB adsorption was investigated. The fitness of the adsorption data with different kinetic and isothermal models has been explored. Moreover, the diffusion mechanism of the MB through the adsorbent has been studied using various kinetic models namely; intraparticle diffusion model, D-W diffusion model, and Boyd diffusion model to determine the actual rate-controlling step for MB removal. Finally, the impact of drying the beads to a different degree and the type of water on the adsorption process was studied to evaluate the practicality of the developed adsorbent.

Keywords: Carboxylated alginate beads; Formulation; Dye; Methylene blue; Adsorption; Kinetics; Isotherms

1. Introduction

Textile industries are the primary source of discharging dyes wastewater, which harms both the environment and the mankind.

Seeking for treatment of dye wastewater resulted in the development of full range treatment techniques such as adsorption, ozonation, coagulation, electrochemical oxidation, and photocatalysis. Each method has its drawbacks. Mainly, adsorption suffers from the limitation of the pollutant

* Corresponding author.

[#]Chemistry Department, College of Science, Jouf University, Sakaka 2014, Saudi Arabia.

transfer from the pollutant medium, the thermal destruction needs for high energy while the biological treatment takes a long time to perform. Indeed, due to the satisfaction of many requirements such as ease, efficiency, and economy, the adsorption technique comes at the front [1,2]. Combination of the adsorption technique with other technology such as photo-degradation increases its benefits compared with other individual contaminants' removal strategies [3–5]. Alginate is a linear copolymer of α -l-guluronate (G) and α -d-mannuronate (M), which constitutes 10%–40% of the dry weight of all species of brown algae. Alginate, among other polysaccharides, has been recognized as an adsorbent for different pollutants, has a natural formulation ability through ionic crosslinking with multivalent metal ions to form hydrogels in various physical forms. These gelation properties can attribute to the simultaneous binding of the divalent cations such as Ca^{2+} to different chains of α -l-guluronate blocks (G-blocks). As a result of their configuration, these chains form electronegative cavities, capable of holding the cations via ionic interactions, resulting in cross-linking of the chains into a structure resembling an "egg box" [6–9]. Also, alginate is used as a carrier for encapsulating microbial organisms which can remove dyes [10]. Alginate beads have been investigated in the removal of different dyes [11–13]. Methylene blue, as one of the cationic dyes, presents a challenge and attracts much attention since it is more toxic than anionic dyes to the single cell green algae, *Selenastrum capricornutum*, and fathead minnow, *Pimephales promelas* [14]. Physical and chemical modifications have been tried to increase the applicability of alginate as adsorbent materials. Yin et al. [15] developed sodium alginate (SA) aerogel by vacuum freeze-drying method which first was crossed bonding in an organic solvent. They found that the adsorption property of SA, which has crosslinked in water is irregular and the adsorption amount was approximately 518 mg/g. At the same time, the adsorption of SA on MB after crosslinking in ethanol is regular, and the maximum adsorption capacity of 567 mg/g is reached.

Rocher et al. [16] developed magnetic alginate/activated carbon composite beads for the removal of methylene blue and methyl orange (MO) dyes. Experimental adsorption isotherms illustrated the efficiency of this system. The adsorption kinetics is fast with 180 min needed to reach equilibrium, 50% of MB being adsorbed in 10 min against 17 min for MO. Zhu et al. [17] developed sodium alginate graft poly(acrylic acid-co-2-acrylamide-2-methyl-1-propane sulfonic acid)/kaolin (SA-g-P(AA-co-AMPS)/KL) hydrogel composite for adsorption of four dyes, namely methyl violet (MV), rhodamine 6G (R6G), acid chrome blue K (AK), and xylenol orange (XO). They found that the maximum adsorption capacities of MV, R6G, AK, and XO are 1,361.1; 1,627.8; 563.5, and 312.4 mg/g, respectively. Feira et al. [18] developed a polymeric adsorbent based on sodium alginate (SAG) grafted with polyacrylamide (PAM) (SAG-g-PAM) using an ultrasound-assisted method for MB removal. They found that the dye adsorption was pH dependent, and maximum adsorption capacity (69.13 mg/g) was at pH 10. Salisu et al. [19,20] studied the removal of methylene blue (MB) dye using alginate graft-polyacrylonitrile and alginate graft-polymethyl methacrylate beads. For the alginate graft-polyacrylonitrile, the removal efficiency of the beads

depends on pH. The experimental equilibrium data successfully fitted to the Langmuir isotherm model with the maximum monolayer coverage of 3.51 mg g⁻¹ and adsorption kinetics data have been well fitted by a pseudo-second-order kinetic model [19]. The alginate graft-polymethyl methacrylate beads indicate that the kinetics of the adsorption process was found to follow pseudo-second-order model and the equilibrium data were best described by Langmuir isotherm model, with a maximum monolayer adsorption capacity of 5.25 mg g⁻¹ [20].

The main obvious drawback of the alginate hydrogel beads is the diffusion limitation of the dye molecules to the interior of the beads, which prolonged the removal time and reduced its efficiency. To overcome this, in our previous study [21], surface-functionalized alginate beads with carboxylic groups were prepared through activation by OH groups with p -benzoquinone (PBQ) coupling agent followed by reaction with iminodiacetic acid (IDA). The functionalized beads show a higher affinity towards MB adsorption compared with the native one. A 25% improvement in the dye removal capacity obtained after 60 min. The main advantage of this strategy was that the functionalized beads show a higher adsorption rate for MB. Within 10 min, 80% of MB was removed using functionalized beads compared with 48% of native ones.

In this study, the formulation conditions of the carboxylated alginate beads, namely; alginate concentration, calcium chloride concentration, crosslinking temperature, and beads size, have been studied. Moreover, the kinetic and isothermal studies of the methylene blue adsorption have performed. Finally, the applicability of the developed beads has tested in tap water, and the impact of its water content (dryness) on its efficiency has been investigated.

2. Materials and methods

2.1. Materials

Cationic MB dye, $\text{C}_{16}\text{H}_{18}\text{N}_3\text{SCl}\cdot 3\text{H}_2\text{O}$, supplied from (NICE CHEMICALS Pvt. Ltd., COCHIN). The stock dye solution prepared by dissolving 50 mg of MB in 1,000 mL distilled water to obtain 50 mg/L (50 ppm) initial dye concentrations. Sodium alginate (NaALG) with a medium viscosity supplied from Sigma-Aldrich Chemicals Ltd. (Germany). Calcium chloride (CaCl_2) provided from Riedel-de Hean Company (Seeize, Germany).

2.2. Methods

2.2.1. Carboxylated alginate beads preparation

The carboxylated alginate beads prepared according to the method mentioned elsewhere [21]. In brief, sodium alginate dissolved in hot distilled water with stirring to have a homogenous solution then dropped 20 mL into 2% calcium chloride solution at room temperature with gentle stirring for 10 min using 25 mL injection syringe with different needle sizes to have two beads size with 1.5 and 3.5 mm diameter. The alginate beads were washed several times using hot distilled water to remove excess calcium chloride. Then reacted with 100 mL of 0.01 M PBQ solution for 5 min at room temperature (RT). The PBQ activated beads were washed several times using hot distilled water to remove

excess PBQ then finally reacted with 100 mL of 0.25% IDA solution (pH 12) for 10 min at RT to have alginate–IDA activated beads which were filtered and washed with distilled water to remove un-reacted IDA. The proposed mechanism was presented in Fig. 1.

2.2.2. Dye adsorption

Adsorption experiments were conducted using conditions mentioned previously unless otherwise stated [21]. In brief, 20 mL beads of 2% alginate concentration (0.4 g dry weight) mixed with 50 mL of 50 mg L⁻¹ MB solution at room temperature at 250 rpm. The adsorption experiment was conducted over 90 min, while the MB concentration was measured using spectrophotometer at λ max of 665 nm and the dye removal (%) was calculated according to the relation:

$$\text{Dye removal (\%)} = \left[1 - \left(\frac{C}{C_0} \right) \right] \times 100 \quad (1)$$

where C_0 is the initial concentration of the dye and C is the concentration at time t .

The uptake capacity is calculated according to the following formula:

$$q_e (\text{mg/g}) = V \frac{(C_0 - C_t)}{M} \quad (2)$$

where q_e is the uptake capacity (mg/g); V is the volume of the MB solution (mL), and M is the mass of the carboxylated alginate beads (CAB) (g).

3. Results and discussion

3.1. Carboxylated alginate beads formulation

Conditions affecting the formulation process of the CAB, namely alginate concentration, calcium chloride concentration, temperature of calcium chloride solution, and beads size, have been investigated.

3.1.1. Alginate concentration

Four concentrations of alginate solution were used to formulate 1.5 mm CAB; 0.5%, 1.0%, 1.5%, and 2%. The impact of initial alginate concentration variation on the adsorption capacity and the dye removal (%) of MB from 30 ppm synthetic solution have been monitored over 120 min at RT and presented in Figs. 2a and b. From Fig. 2a, it can be seen that the dye removal (%) increased from 67% to 84% with increasing the alginate concentration from 0.5% to 2%. The adsorption capacity showed a reverse behaviour, which decreased from 10.05 mg/g for 0.5% alginate beads to 3.15 mg/g for 2.0% alginate beads (Fig. 2b). The equilibrium established in a reasonably short time from 20 min of 0.5% alginate beads to 45 min of 2.0% alginate beads. Increasing the alginate concentration leads automatically to increase the number of adsorption sites available to MB molecules, which in turn leads to decrease the adsorption capacity. On the other hand, the density of the alginate beads increased with the increase of the alginate concentration which creates, in turn, a diffusion barrier to the MB molecules to reach the interior pores of the alginate beads. That consequently reflected on the prolongation of the equilibrium time.

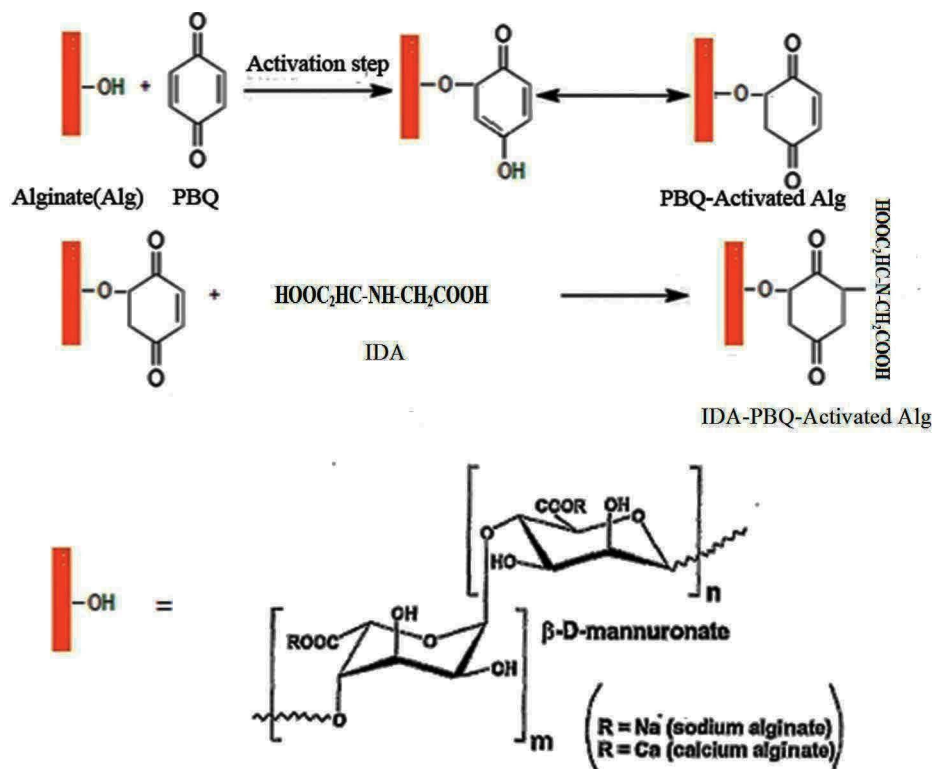


Fig. 1. Proposed mechanism of alginate functionalization with IDA.

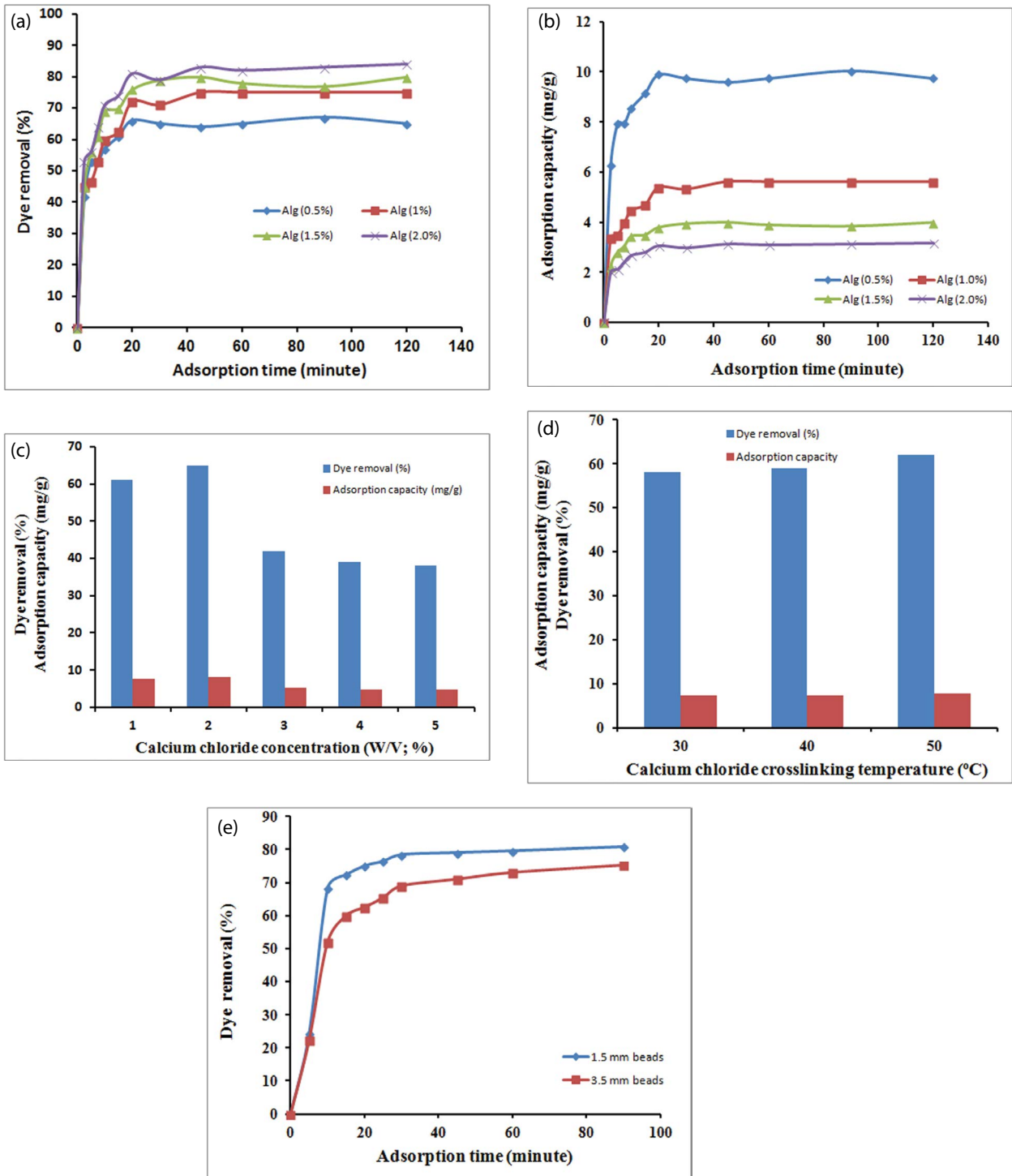


Fig. 2. Effect of (a) alginate concentration on the MB adsorption capacity using CAB, (b) alginate concentration on MB removal percentage using CAB, (c) calcium chloride concentration on the MB adsorption capacity and removal percentage using CAB, (d) calcium chloride crosslinking temperature on the MB adsorption capacity and removal percentage using CAB, and (e) CAB size on the MB adsorption capacity and removal percentage.

3.1.2. Calcium chloride concentration

The effect of variation of the concentration of the calcium chloride crosslinking solution on the adsorption capacity and the MB removal (%) from 100 mL of 50 ppm synthetic

solution have been monitored for 60 min at RT and presented in Fig. 2c. From Fig. 2c, it can be seen that the dye removal (%) of MB slightly increased from 61% to 65% with the increase of the crosslinker concentration from 1% to 2% where maximum dye removal (%) detected. Any further

increment of the crosslinker concentration reduced the dye removal (%) of MB to 42%, 39%, and 38% for 3%, 4%, and 5%, respectively. The adsorption capacity of the CAB shows the same behaviour. Consumption of the carboxylate groups of the glucose ring in the ionic crosslinking process with calcium ions may explain the demonstrated behaviour. The negatively charged carboxylate groups on alginate structure acting as an active site for adsorbing MB through opposite charge attraction. In the same time, the carboxylate groups were incorporated in the ion crosslinking gelation process to form the beads with calcium ions. Such competition behaviour between calcium ions and MB molecules resulted in reducing the active sites, inside the core of the alginate beads, available for MB adsorption and increase the crosslinking of the beads creating diffusion barrier retarded the reach of the MB molecules from the bulk solution to reach the remaining free carboxylate groups in the beads interior [21].

3.1.3. Calcium chloride ionic crosslinking solution temperature

The effect of variation of the calcium chloride crosslinking solution temperature, from 30°C to 50°C, on the adsorption capacity and the MB removal (%) from 100 mL of 50 ppm synthetic solution have been monitored over 60 min (Fig. 2d). The results obtained indicated that a small effect had been noticed where the dye removal (%) was 58%, 59%, and 62% at 30°C, 40°C, and 50°C, respectively. On the other hand, the adsorption capacity increased slightly 7.25, 7.375, and 7.75 mg/g at 30°C, 40°C, and 50°C, respectively. The obtained results may be explained by the adsorption process mainly on the carboxylate groups located on the surface which did not incorporate the ionic crosslinking step of the beads where very fast adsorption has been observed at the first 10 min then levelling off started to appear in Fig. 2 [21].

3.1.4. Bead size

Two CAB sizes have been prepared, 1.5 and 3.5 mm, to explore the effect of variation of the size of the bead on the adsorption capacity and the MB removal %. Experiments performed using 50 mL of 30 ppm and monitored over 90 min at RT. Depicting the results shown that quick initial adsorption step has been observed after only 10 min where 70% and 52% of MB has been removed using 1.5 mm beads and 3.5 mm beads. The equilibrium has been almost reached after only 30 min of 1.5 mm beads while takes longer time, 60 min, of 3.5 mm beads. Overall, the dye removal percentages found 81% and 75% of 1.5 and 3.5 mm beads (Fig. 2e). The adsorption capacity was found to be very close, that is, 3.03 and 2.82 mg/g for 1.5 and 3.5 mm beads. The higher surface of the 1.5 mm alginate beads, the higher number of carboxylate groups on the surface of the beads, may explain the higher rate of removal in the early stage of the adsorption process. With the progress of the adsorption process, the concentration gradient between the MB molecules concentration in the liquid phase and on the surface of the beads starts to decrease which is the driving force of the MB molecules movement from the liquid phase to the solid phase (alginate beads) [21].

3.2. Dye adsorption

3.2.1. Effect of methylene blue concentration

The result of variation of the MB concentration from 7 to 53 ppm on the adsorption capacity and the MB removal (%) has been explored using 1.5 mm alginate beads over 60 min adsorption time (Fig. 3a). It can be seen that the adsorption capacity increased linearly while the dye removal % increased linearly up to 30 ppm then started to level off. The increment of the adsorption capacity is in agreement with results obtained by Zhu et al. [17]. They claimed that there are strong electrostatic forces between the negatively charged groups such as $-\text{COO}^-$ and $-\text{SO}_3^-$ on the sodium alginate graft poly(acrylic acid-co-2-acrylamide-2-methyl-1-propane sulfonic acid)/kaolin (SA-g-P(AA-co-AMPS)/KL) hydrogel composite and the positively charged groups on the dye molecules. Thus, the adsorption amounts significantly enhanced as the dye concentrations increased. A similar trend has been found by Salisu et al. [19,20] in the removal of MB dye using PAN grafted alginate and PMMA grafted alginate beads. However, different behaviour of the removal percentage was found by them where they detected the maximum percentage removal occurred at 6 ppm concentration with maximum percentage removal of 85.34% and 65% then steadily decreased. They referred to the saturation of the adsorption sites on the adsorbent surface, which indicates the possibility of the formation of monolayer coverage of the dye molecules at the interface of the adsorbent. The obtained behaviour in this work is different, which may reflect a higher number of adsorption sites.

3.2.2. Effect of the contact time

The influence of elapsing the adsorption time on the adsorption capacity and the MB removal (%) has been shown in Fig. 3b. From the figure, it is evident that the dye removal (%) increased rapidly in the first 15 min, where 79% of the MB has been removed. Fast equilibrium within 30 min was achieved with 86% of the MB removed. The adsorption capacity shows a similar trend. Zhu et al. [17] had the same observation. According to them, this was due to the fast spread of the networks of the adsorbent at the early stage. As a result, it was much easier for dye molecules to penetrate the inside of the resin and combine with the adsorption sites [22]. With the extension of time, the active groups on the surface of the adsorbent became less, and the adsorption approached equilibrium.

3.2.3. Effect of the adsorbent amount

Figs. 3c and d show an apparent influence of the adsorbent amount on the adsorption parameters. Only 5 min are enough to remove 77% of the MB (50 mg/L) using 0.4 g adsorbent while 45 min are required to have the same removal percentage using 0.1 and 0.2 g adsorbent. The equilibrium time shifted to be shorter with a higher amount of the adsorbent due to the increase of the surface carboxylate groups sites available for MB adsorption (Fig. 3c). As a result, the highest adsorption capacity recorded for 0.1 g adsorbent; 19 mg/g while reduced with increase the adsorbent amount to reach 9.85 and 5.33 mg/g for 0.2 and

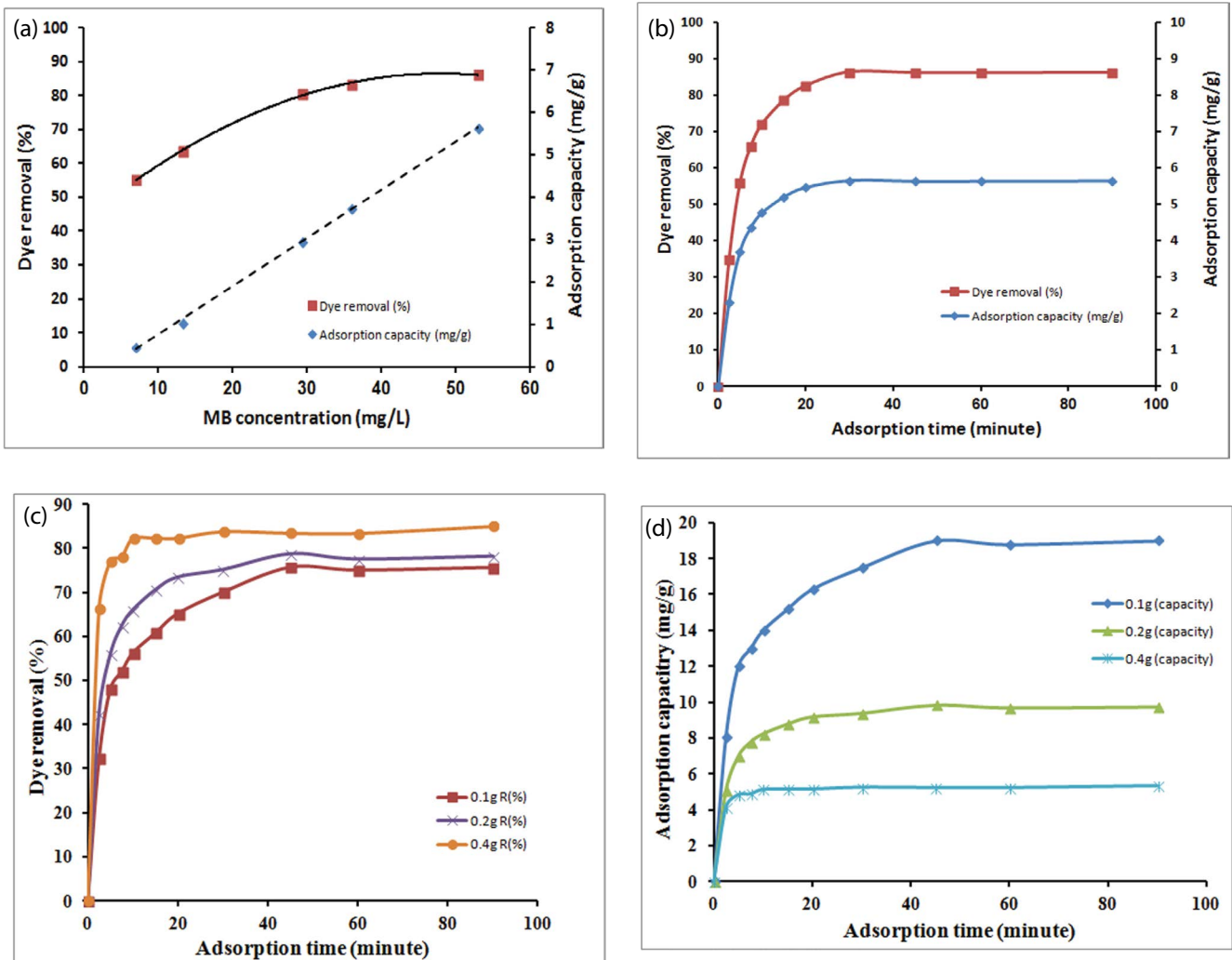


Fig. 3. Effect of (a) MB concentration on the MB adsorption capacity and removal percentage using CAB, (b) contact time on the MB adsorption capacity and removal percentage using of CAB, (c) adsorbent amount on the MB adsorption capacity using of CAB, (d) adsorbent amount on the MB removal percentage using of CAB.

0.4 g adsorbent (Fig. 3d). This finding expected, and the following results are found by other authors since the MB solution contains a fixed amount of MB molecules while different numbers of active sites are available over the adsorbent surface [13,17].

3.2.4. Adsorption kinetic models

The adsorption data obtained in Fig. 6 fitted using different kinetic models namely the pseudo-first-order [23], the pseudo-second-order [24], and the Elovich [25] to explore the kinetics of the MB adsorption process over CAB beads using linear form Eqs. (3)–(5), respectively, and presented in Fig. 4.

$$\ln(q_e - q_t) = \ln q_e - k_1 t \tag{3}$$

$$\frac{t}{q_t} = \left(\frac{1}{k_2 q_e^2} \right) + \frac{t}{q_e} \tag{4}$$

$$q_t = \alpha + \beta \ln t \tag{5}$$

q_e and q_t are the amounts of ions adsorbed (mg/g) at equilibrium and time t (min), respectively. k_1 (min^{-1}) is the first-order reaction rate constant. k_2 is the second-order reaction rate equilibrium constant (g/mg min). α represents the initial sorption rate (mg/g min), and β is related to the extent of surface coverage and activation energy for chemisorption (g/mg).

Extracted from Fig. 4, the adsorption parameters of the kinetic models are tabulated in Table 1. From the table, it is evidenced that the correlation coefficients of the data fitting are 0.9991, 0.9935, and 0.8259 for the pseudo-second-order, the pseudo-first-order, and the Elovich models, respectively. The pseudo-second-order model best fitting the adsorption data where the value of $q_{e, \text{calculated}}$ (5.8411 mg/g) is the closest to the experimental value (5.65 mg/g). Hence, it suggests that the rate-limiting step in these sorption processes may be chemisorptions involving sufficient forces through the sharing or exchanging of electrons between sorbent

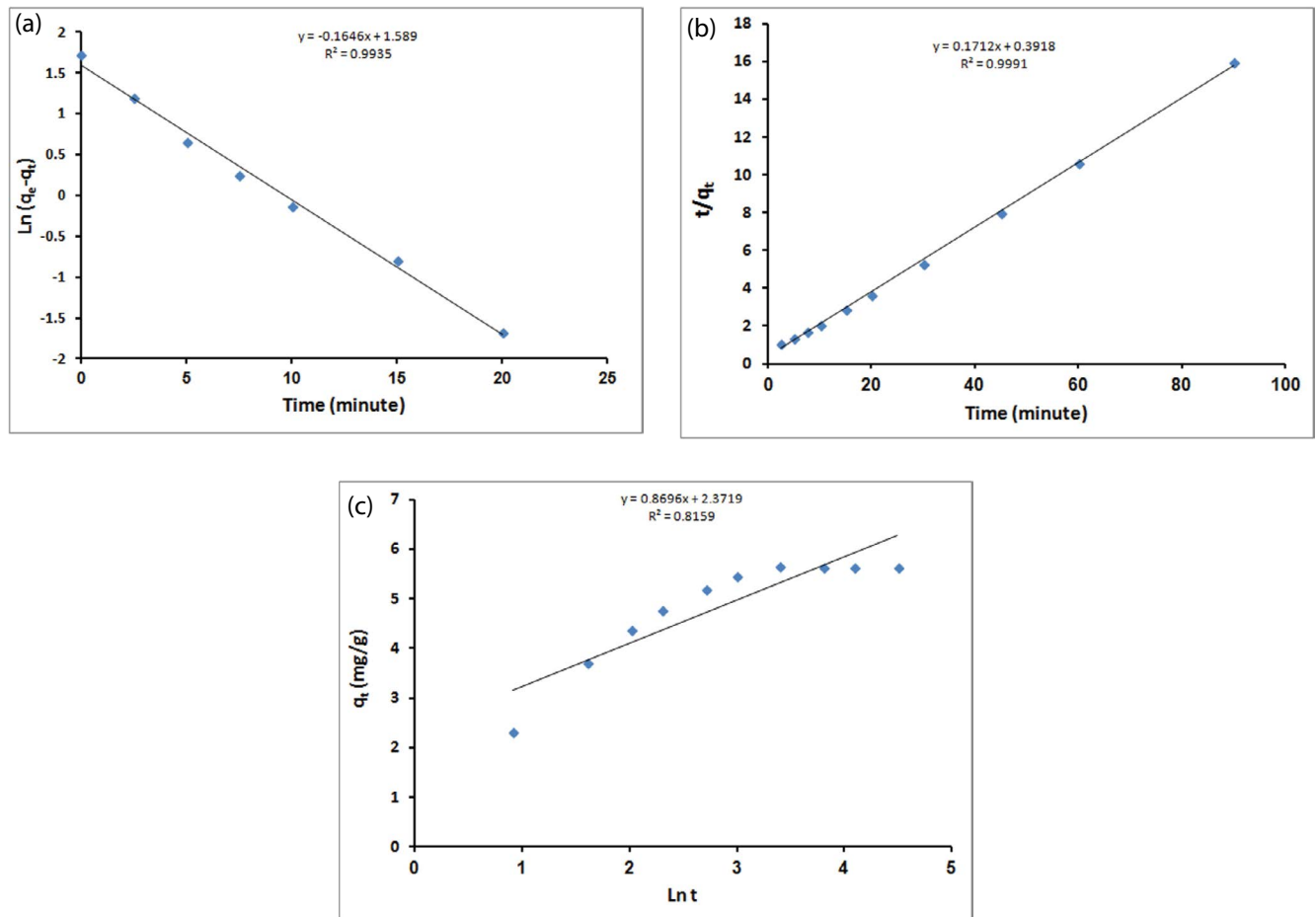


Fig. 4. Adsorption kinetic models for MB removal using CAB: (a) first order plots, (b) second order plots and (c) simple Elovich plots.

Table 1

Adsorption parameters of the pseudo-first, the pseudo-second-order and the Elovich kinetic models

Pseudo-first-order				Pseudo-second-order			Elovich		
$q_{e,exp.}$ (mg/g)	$q_{e,cal'}$ (mg/g)	K_1 (min ⁻¹)	R^2	$q_{e,cal}$ (mg/g)	K_2 (m ² mg ⁻¹ min ⁻¹)	R^2	β (g/mg)	α (mg/g min)	R^2
5.65	4.899	0.1646	0.9935	5.8411	0.3918	0.9991	0.8696	2.3719	0.8159

and sorbate [26]. The value of β (0.8696 g/mg) is indicative of the number of sites available for removal while α (2.3719 mg/g min) is the removal quantity when $\ln t$ is equal to zero; that is, the removal quantity when t is 1 h giving insight about the removal behaviour of the first step [27].

3.2.5. Adsorption mechanisms models

The description of the diffusion process of MB ions from the liquid phase (solution) to the solid phase (adsorbent) performed using three kinetic models. Two models, namely Dumwald–Wagner and intraparticle models, described the liquid film diffusion or intraparticle diffusion [28,29] while the external mass transfer was examined by Boyd model.

The linear form of equations determined the diffusion rate inside particulate using the Dumwald–Wagner model

[30] and the intraparticle model [31] presented in Eqs. (6) and (7).

$$\log(1 - F^2) = -\left(\frac{K}{2.303}\right) \times t \quad (6)$$

$$q_t = k_d t^{1/2} + C \quad (7)$$

where K is the diffusion rate constant and the removal percentage, F is calculated by (q_t/q_e) . The intraparticle diffusion rate is k_d and the thickness of the boundary layer is represented by C .

Fig. 4. presents fitting of the adsorption data shown in Fig. 3b using the Dumwald–Wagner and the intraparticle models; Figs. 5a and b. From the figure, it is clear that the Dumwald–Wagner fitted the adsorption data very well

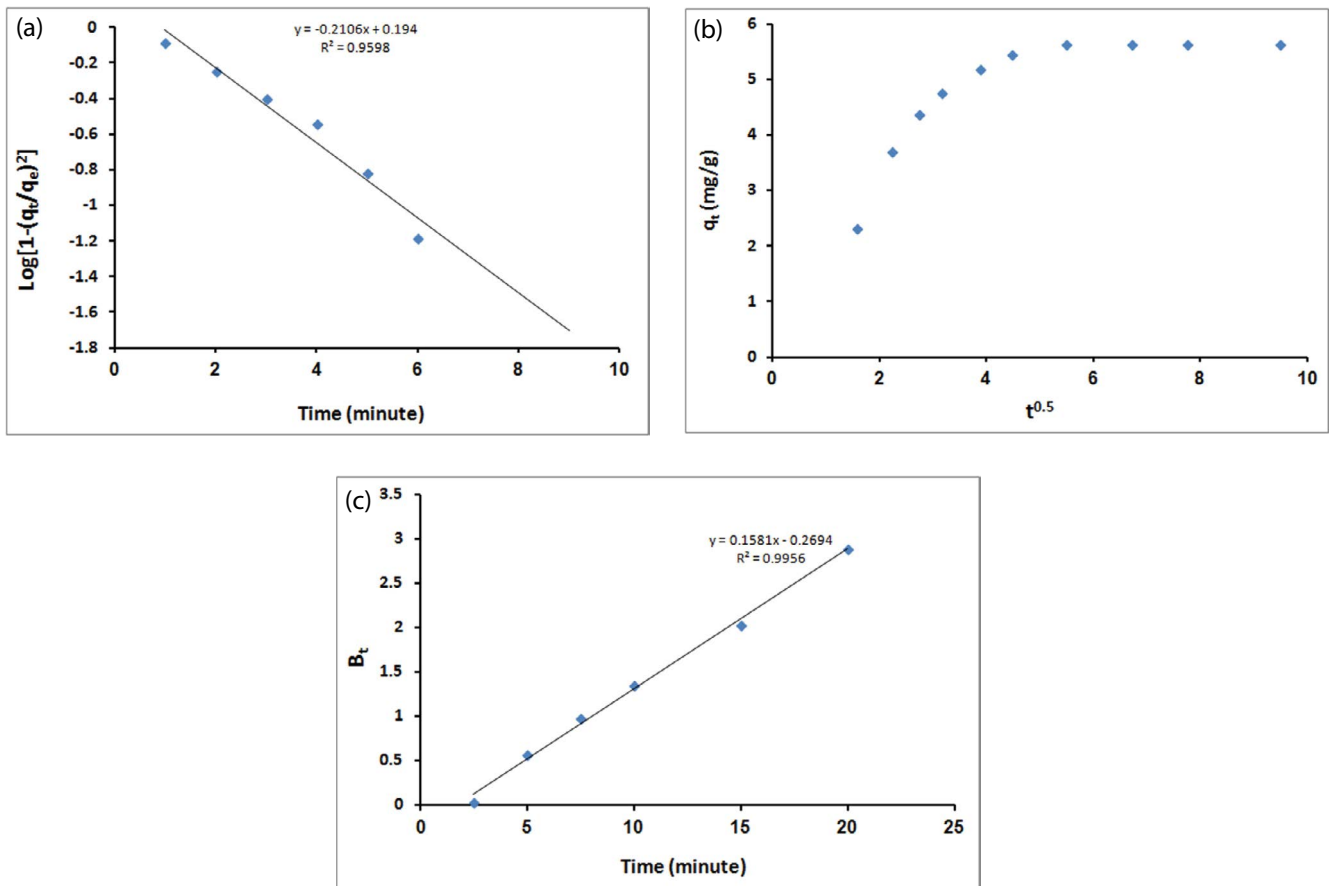


Fig. 5. Adsorption mechanisms models of MB removal using CAB: (a) Dumwald–Wagner plots for intraparticle diffusion, (b) Intraparticle diffusion plots, and (c) Boyd expression.

($R^2=0.9598$), and the diffusion rate constant K is found to be 0.4850 min^{-1} .

The adsorption data fitting using the intraparticle diffusion model in Fig. 5b show two separate linear portions suggesting that the removal process consists of both surface removal and intraparticle diffusion. While the initial linear part of the plot is the indicator of the boundary layer effect, the second linear portion is due to intraparticle diffusion [32]. The intraparticle diffusion rate (k_d) is $0.0611 \text{ mg}/(\text{g min}^{1/2})$, and the thickness of the boundary layer (C) value is 5.1506 , the larger the intercept, the higher is the boundary layer effect [33].

The actual rate-controlling step involved in the MB sorption process determined by further analysis of the sorption data by the kinetic expression is given by Boyd et al. [34].

$$F = 1 - \left(\frac{6}{\pi^2}\right) \exp(-B_t) \tag{8}$$

$$F = \frac{q}{q_\alpha} \tag{9}$$

$$B_t = -0.4978 - \ln\left(\frac{1-q}{q_\alpha}\right) \tag{10}$$

q and q_α represent the amount sorbed (mg/g) at any time t and at an infinite time (in the present study 30 min). F is the fraction of MB adsorbed at different time t given by Eq. (9) and B_t is a mathematical function of F . With substituting Eq. (8) into Eq. (9), we obtained the kinetic expression presented in Eq. (10).

According to Eq. (10), the data fitted in Fig. 5c and useful information to distinguish between external-transport and intraparticle-transport controlled rates of sorption can extract. From the linearity of this plot which did not pass through the origin we can conclude that the film diffusion governs the rate limiting process [35]. The aromatic hydrophobic groups of r-benzoquinone play a significant role in changing the hydrophilic–hydrophobic balance of the CAB beads and accordingly the thickness of the formed liquid boundary layer over the solid surface. That leads to make the film diffusion is the limiting process [36].

3.2.6. Adsorption isotherm models

The equilibrium adsorption data presented in Fig. 3a was fitted using different adsorption isotherm models such as Freundlich, Langmuir, Temkin and Dubinin–Radushkevich models; Fig. 6.

The most applicable models are the Langmuir and Freundlich where the first assumes completely homogeneous

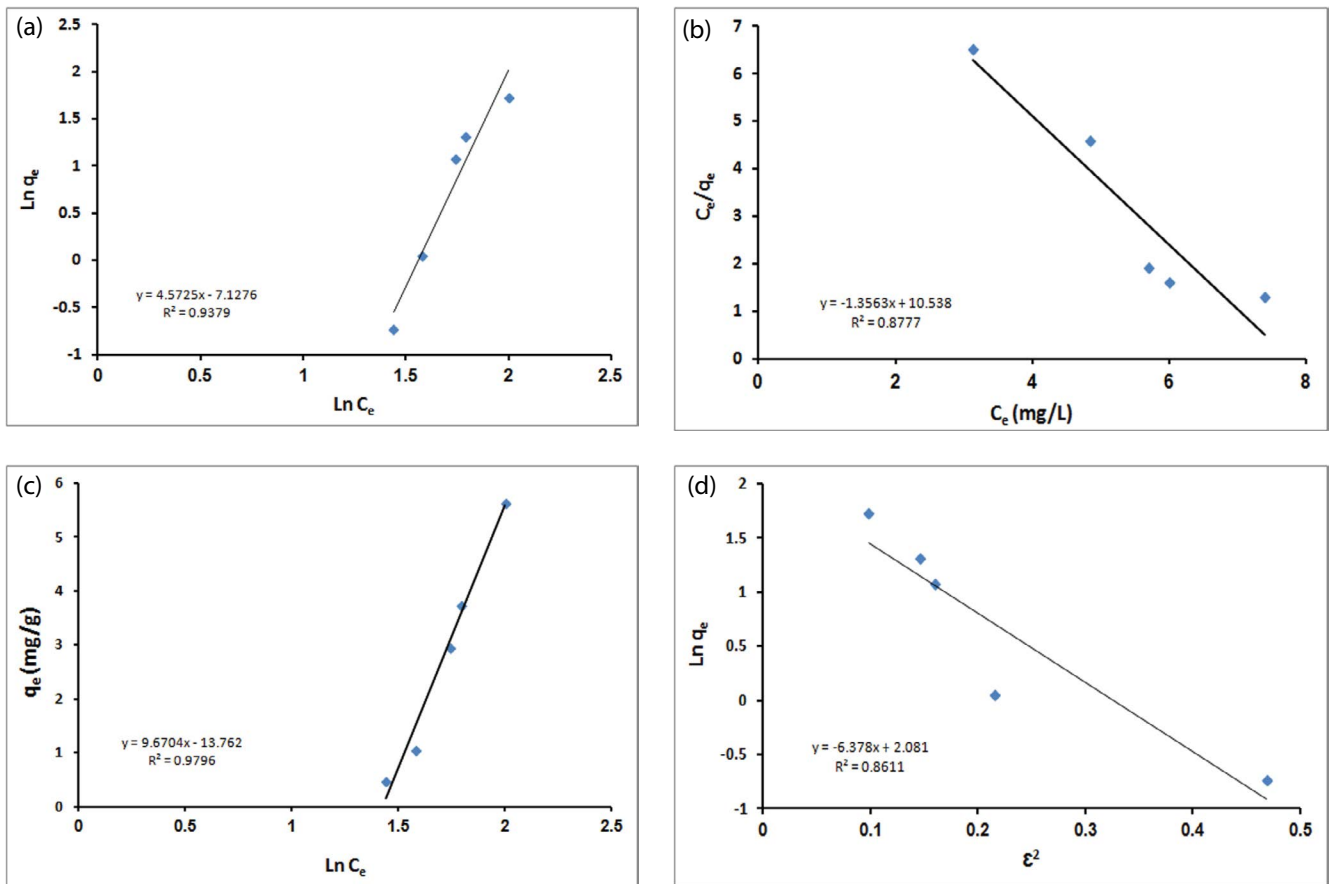


Fig. 6. Adsorption isothermal models for MB removal with various initial solution concentrations using CAB: (a) Freundlich isotherm, (b) Langmuir isotherm, (c) Temkin isotherm, and (d) D–R isotherm.

surface with a finite number of identical sites and with a negligible interaction between adsorbed molecules which results in monolayer sorption while the second postulate heterogeneous surfaces site energies and multi-layer levels of sorption [37,38].

The linear formula for Freundlich [39,40] and Langmuir [41], is expressed as Eqs. (11) and (12).

$$\ln q_e = \ln K_F + \frac{1}{n_f} \ln C_e \quad (11)$$

$$\frac{C_e}{q_e} = \frac{1}{q_m K} + \frac{C_e}{q_m} \quad (12)$$

q_e (mg/g) is the adsorbent capacity, and C_e (mg/L) is the adsorbate concentration at equilibrium. K_F and n_f Freundlich constants indicated the adsorption capacity and adsorption intensity. q_m is the maximum monolayer adsorption capacity (mg/g), and K is the adsorption energy (L/mg).

Fig. 6a presents linear fitting, correlation coefficient (R^2) value (0.9379), of the adsorption data using the Freundlich equation. From the figure, it can be seen that the amount of MB adsorbed over the adsorbent surface increases as long as there is an increase in the MB concentration. The value

of Freundlich constant n_f (0.2187) which is <1 dictates unfavourable sorption for MB with the CAB beads [40].

On the other hand, Fig. 6b illustrates a linear plot of the adsorption data using the Langmuir equation; R^2 value is 0.8777. From the figure, the calculated value of q_m is 0.7373 mg/g. The value of K is 7.77 L/mg, which indicates that the CAB was moderately efficient for MB removal since it had moderately low energy of sorption and affinity towards MB.

Dimensionless separation factor (R_L) that is used to predict the favourability of the adsorption system was calculated using Eq. (13) [42]:

$$R_L = \frac{1}{(1 + KC_0)} \quad (13)$$

C_0 is the MB initial concentration (mg/L). The calculated values of R_L for MB removal (Table 2) show favourable removal because the R_L values ranged between 0.0 and 1.0 [43,44]. That values again confirm that the Langmuir isotherm was convenient for the sorption of MB onto CAB which agreed with the obtained results by Mohy Eldin et al. [45] of the removal of MB using phosphoric acid-doped pyrazole-g-poly(glycidyl methacrylate) particles.

Other isotherm models compromise between the Freundlich and Langmuir isotherm models such as the Temkin

Table 2
The R_L values for different initial MB concentrations

C_0	R_L
7	0.018
13.3	0.0096
29.4	0.00436
36	0.00356
53	0.00242

isotherm. The Temkin isotherm takes into account the impact of indirect adsorbent/adsorbate interactions on the adsorption process, which reduced the heat of adsorption of all molecules in a layer [46] linearly. That can be expressed in a linear form as follows [47]:

$$q_e = B \ln K_T + B \ln C_e \tag{14}$$

K_T is the Temkin equilibrium binding constant corresponding to the maximum binding energy, and B is the Temkin constant related to the heat of sorption extracted from the linear plot in Fig. 6c and presented in Table 3.

The D-R isotherm is more general than the Langmuir isotherm, where it refused the surface homogeneity or the constant of the adsorption potential [40]. The D-R isotherm is expressed as follows:

$$\ln q_e = \ln V'_m - K'\epsilon^2 \tag{15}$$

where q_e is the mg of MB removed per g of CAB, V'_m is the D-R sorption capacity (mg/g), K' is a constant related to the adsorption energy (mol^2/kJ^2), and ϵ is the Polanyi potential. ϵ is calculated with the following equation:

$$\epsilon = RT \left(1 + \frac{1}{C_e} \right) \tag{16}$$

where R is the gas constant ($8.314 \times 10^{-3} \text{ kJ/mol K}$), and T is the temperature (K). The constant K' gives the mean free energy of sorption per molecule of the sorbate (E) when it is transferred to the surface of the solid from infinity in the solution.

This energy gives information about the physical and chemical features of the sorption process [44] and can compute with the following relationship [48]:

$$E = (2K')^{-0.5} \tag{17}$$

E is the amount of energy required to transfer 1 mole of the MB from the bulk solution to the CAB surface which indicates following a chemical ion exchange mechanism If E is between 8 and 20 kJ/mol or a physical nature if $E < 8$ kJ/mol [49,50].

Plotting the adsorption data is given in Fig. 6d, where a straight line is obtained; R^2 0.8611. From the figure, the calculated adsorption energy ($E < 8$ kJ/mol) indicates that the MB sorption processes could be considered physisorption in nature [51]. Therefore, it is possible that physical means such as electrostatic forces played a significant role as sorption mechanisms for the sorption of MB in this work.

The parameters and the correlation coefficients of the Langmuir, the Freundlich, the Temkin and the Dubinin–Radushkevich (D-R) isotherm models applied to MB sorption on CAB are summarized in Table 3. From the table, it is clear that the Temkin isotherm model yielded the highest R^2 value (0.9796), and this showed that MB sorption on the polymer is described well by this model which considers the impact of indirect adsorbent/adsorbate interactions on the adsorption process which reduced the heat of adsorption of all molecules in a layer linearly.

3.3. Applicability

3.3.1. Effect of water type

To examine the applicability of the developed CAB, the adsorption of MB from synthetic aqueous solution (30 ppm) prepared using both distilled and tap waters were followed over 60 min at RT. The adsorption capacity and the dye removal % are detected and presented in Table 4. From the figure, it is clear that no significant effect was observed. This finding is an advantage which eliminates the possibility of interactions caused by the dissolved salts in tap water.

3.3.2. Effect of beads water content (beads drying time)

The storage of the prepared CAB at RT for further usage may have an impact on its efficiency of MB adsorption. The CAB was left to dry for 1, 3, 4, 5, and 24 h at RT and then tested for removal of MB from 50 mg/g synthetic solution. The adsorption capacity and the dye removal (%) monitored, Table 5. From the table, it is evident that drying of the beads for 3 h negatively affected both the adsorption capacity and the dye removal %, which reduced to 7.7 mg/g and 61.56%, respectively. Meanwhile, a positive impact is noticed in case of drying the beads for 4 h where the adsorption capacity and the dye removal % were found to be increased to 8.75 mg/g and 70%, respectively. This improvement shows best results at 5 h drying where the adsorption capacity

Table 3
Parameters and the correlation coefficients of Langmuir, Freundlich, Temkin and Dubinin–Radushkevich (D-R) isotherm models

Langmuir isotherm			Freundlich isotherm			Temkin isotherm			Dubinin–Radushkevich (D-R)			
q_{\max} (mg/g)	K_L (L mg ⁻¹)	R^2	K_f (mg/g)	n_f	R^2	B_T (J/mol)	K_T (L/g)	R^2	K (mol ² /kJ ²)	V_m (mg/g)	E (kJ/mol)	R^2
0.7373	7.77	0.8777	0.0008	0.2187	0.9379	9.6704	0.2409	0.9796	-6.378	8.012	0.2799	0.8611

and the dye removal (%) reached to 9.21 mg/g and 73.7%. Drying the beads for 24 h drastically reduced the adsorption capacity and the dye removal % to 4.95 mg/g and 39.6%. That reduction of the 24 h dried CAB adsorption parameters gave useful information about the percentage of the adsorption sites located in the pores of the CAB.

The data have been applied using the intraparticle model; Fig. 7. Two separate linear portions represent 5 h dried bead curve observed. These two linear portions in the intraparticle model suggest that the removal process consists of both surface removal and intraparticle diffusion. The presence of only one line portion in case of 24 h dried beads confirms the absence of the intraparticle diffusion and the process is controlled only by surface diffusion. The simple calculation gave us an indication that 46% of the removal process occurs in the pores of the CAB.

3.4. Comparative study

Table 6 presents a comparative study of the MB removal using alginate hydrogel with physical and/or chemical modifications. Also, different other natural adsorbents were included. From the table, it is clear that the alginate hydrogel adsorbents have a varied range of adsorption capacity depending on the physical or chemical modification performed. Alginate grafted hydrogel, using hydrophobic polymers, such as PAN-g-Alginate [19] and PMMA-g-Alginate [20] have deficient adsorption capacity; 3.51 and 5.25 mg/g. The grafting of alginate with a hydrophilic polymer such as PAM-g-Alginate [18] has a positive effect on its adsorption capacity, which increased to be 69.13 mg/g. Increase in the surface area of adsorption as physical modification has a pounced impact which increased the adsorption capacity tremendously as in case of Ca-Alginate gas gel (518–567 mg/g) [15] and porous alginate (1,426 mg/g) [52]. Other natural based adsorbents such as *Hibiscus cannabinus*-g-PAA and *Hibiscus cannabinus*-g-PAA/PAAM show low adsorption capacity (7.0 mg/g) [53] regardless of grafting with functional polymers. Activated lignin–chitosan blends and brown macroalga show moderately medium adsorption capacity (35–36 mg/g) [54,55]. Inorganic adsorbent such as MOF has moderately high adsorption capacity (326 mg/g) [56]. Our carboxylated alginate beads show a promising adsorption capacity, especially in case of decreased size and drying of the bead. Increase in the surface area through increase in the porosity will significantly improve the adsorption capacity and shorten the adsorption time.

Table 4
Effect of water type on the adsorption capacity and dye removal (%)

Time (min)	Dye removal (%)		Adsorption capacity (mg/g)	
	Distilled water	Tap water	Distilled water	Tap water
5	56	54	2.1	2.025
10	70.75	66	2.65	2.48
15	73.35	68	2.75	2.55
20	74.25	70.44	2.78	2.64
45	79.7	77.15	2.99	2.90
60	79.7	78.9	2.99	2.96

Table 5
Effect of the drying time on the adsorption capacity & dye removal (%)

Time (hour)	Adsorption capacity (mg/g)	Dye removal (%)
0	8.22	65.73
1	7.02	56.14
3	7.7	61.56
4	8.75	70.00
5	9.21	73.70
24	4.95	39.60

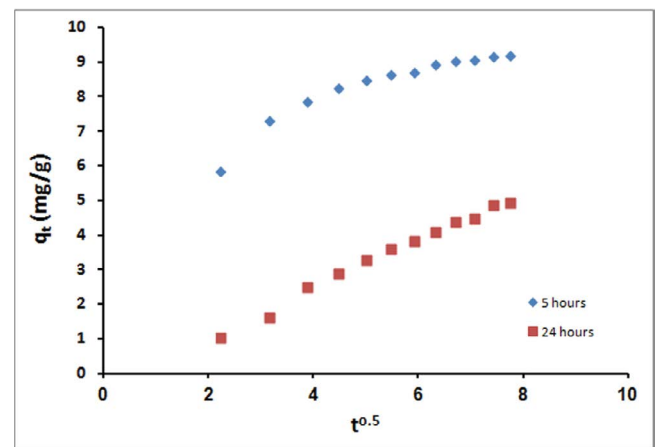


Fig. 7. Intraparticle diffusion plots for MB removal using dried CAB.

3.5. Polymer matrices characterization

3.5.1. FT-IR analysis

The FT-IR spectra of alginate, IDA-functionalized alginate (IDA-Alg), and MB-adsorbed IDA-functionalized alginate (MB-IDA-Alg) were investigated. All alginate forms showed broad band between 3,000 and 3,700 cm^{-1} , which attributed to O–H stretching vibrations. The spectrum of alginate (Fig. 8a) showed the peaks at around 2,937; 1,590; 1,412 and 1,020 cm^{-1} , indicating the stretching vibrations of aliphatic C–H, COO^- (asymmetric), COO^- (symmetric), and C–O, respectively, which are characteristics of the polysaccharide [57]. The spectrum of the IDA-Alg showed the

Table 6
Comparison of the MB adsorption capacity of different adsorbents

Adsorbent matrices	Capacity (mg/g)	References
Ca-Alginate gas gel	518–567	15
PAM-g-Alginate	69.13	18
PAN-g-Alginate	3.51	19
PMMA-g-Alginate	5.25	20
Porous alginate	1,426	54
<i>H. cannabinus</i> -g-PAA	7.11	55
<i>H. cannabinus</i> -g-PAA/PAAM	7.00	55
Activated lignin–chitosan blends	36.25	56
Brown macroalga	35.06	57
MOF	326	58
Carboxylated alginate	14	This work

peaks at around 2,930; 1,591; 1,413; and 1,022 cm^{-1} , indicating the stretching of aliphatic C–H, COO^- (asymmetric), COO^- (symmetric), and C–O, respectively. The original bands for IDA at around 1,400; 1,590; and 3,100 cm^{-1} overlapped with the counter ones of alginate where the absorbance increased compared with the alginate. Moreover, a new band compared with alginate spectrum at around 1,740 cm^{-1} was assigned to the carboxylic carbonyl group

of IDA, which confirmed the functionalization of the alginate molecules with IDA [58] (Fig. 8b). The spectra of the MB-adsorbed IDA-functionalized alginate (MB-IDA-Alg) are shown in Fig. 8c. The characteristic bands of the alginate were recognized at 2,930; 1,594; 1,413; and 1,027 cm^{-1} . The typical bands of the MB at 1,598 and 1,391 cm^{-1} overlapped with the counter ones of the IDA-Alg at 1,400 and 1,590 cm^{-1} . The characteristic peak of the carboxylic carbonyl group of IDA at around 1,740 cm^{-1} (Fig. 8b) has disappeared in Fig. 8c due to the adsorption of MB molecules and the characteristic peak of MB at 886 cm^{-1} appeared [59]. According to those results mentioned above, the following sorption mechanisms were proposed:

- Electrostatic interaction between the negative COO^- and the cation groups N^+ of the MB.
- n - π interactions between deprotonated COO^- groups of the sorbent as n -donors with the π acceptor sites of the aromatic ring of the MB [60].
- π - π interactions between π -aromatic ring donors of MB and π acceptor groups in the sorbents (i.e., the aromatic ring of the PBQ) [60].

3.5.2. Thermal gravimetric analysis

Thermogravimetric curves of alginate and IDA-activated alginate beads in a nitrogen atmosphere are displayed in Fig. 9. The thermogram of sodium alginate exhibited two

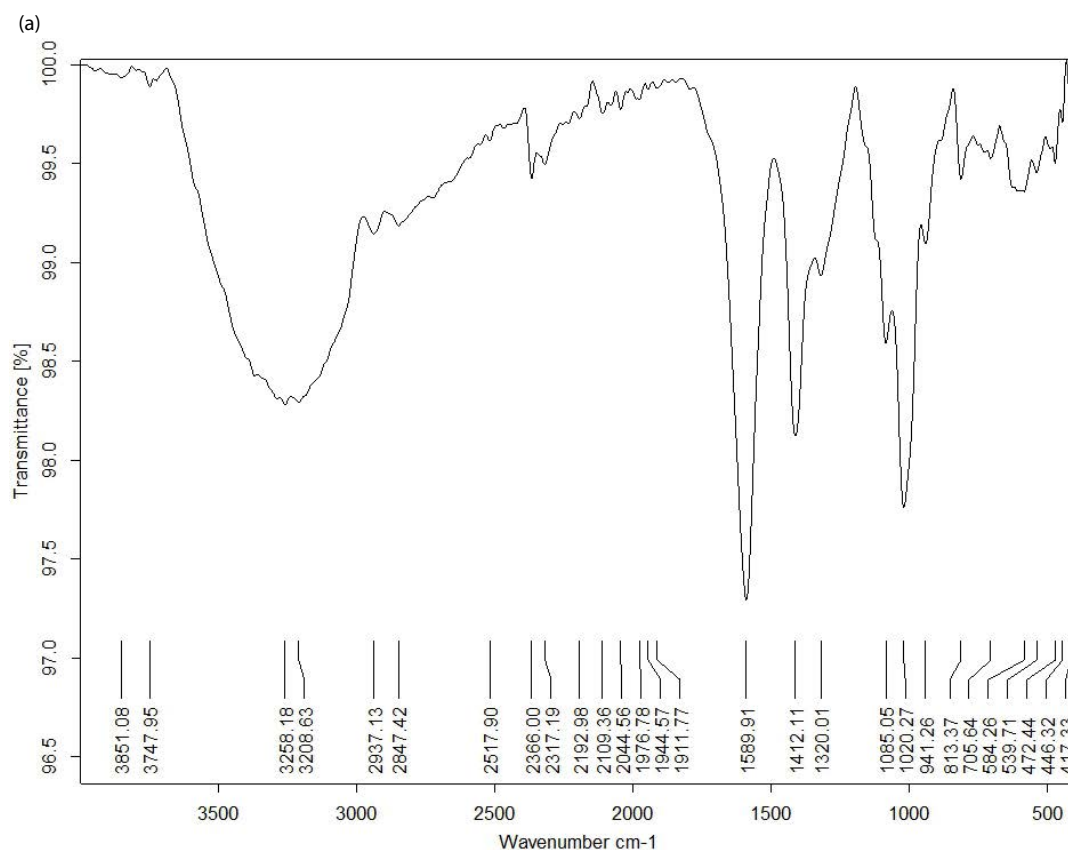


Fig. 8. Continued

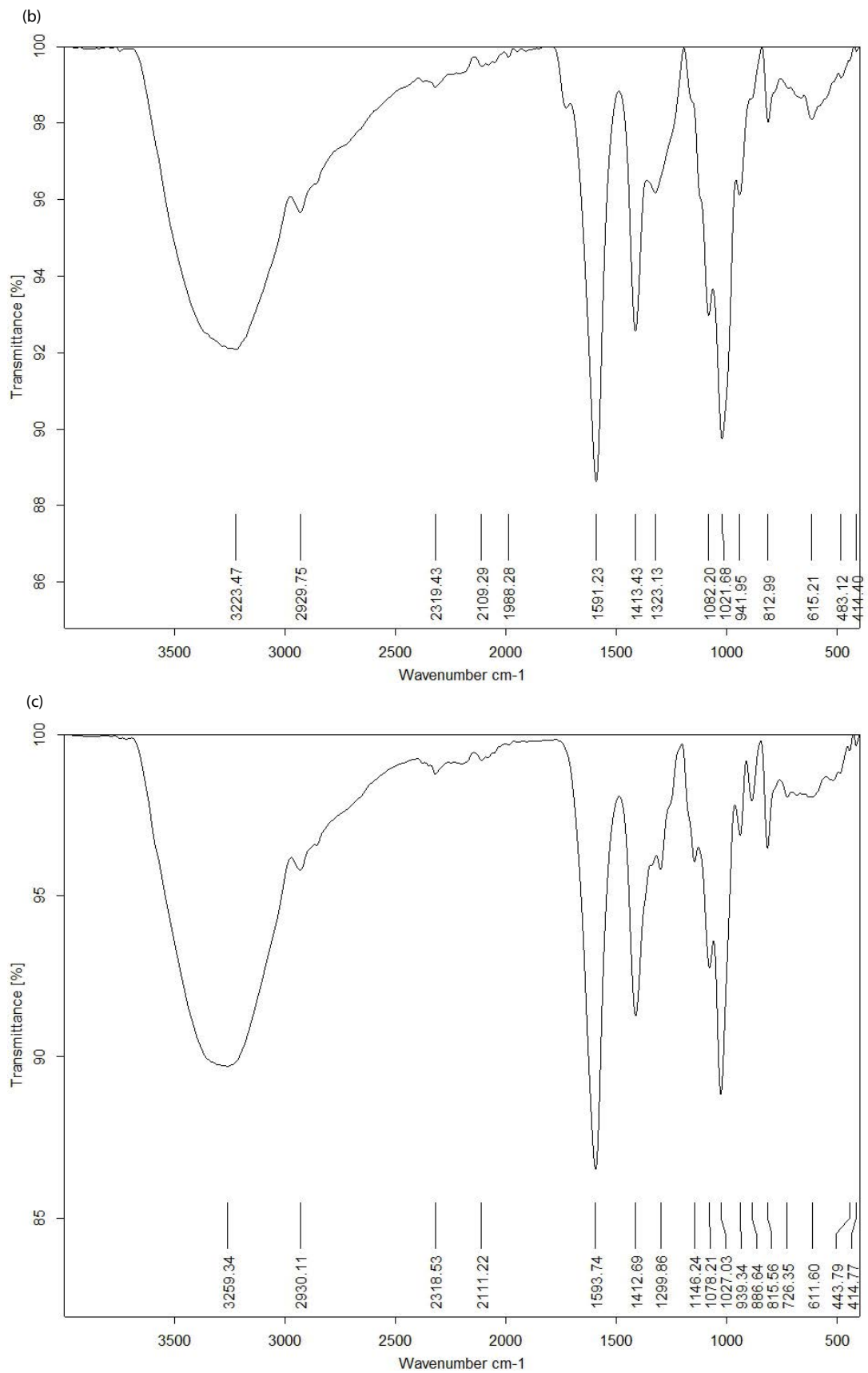


Fig. 8. FT-IR spectra of (a) alginate, (b) IDA-alginate, and (c) MB-IDA-alginate.

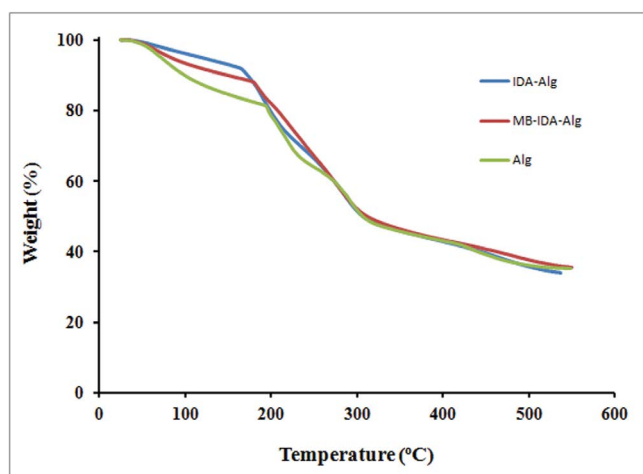


Fig. 9. Thermal gravimetric analysis of alginate, IDA-alginate, and MB-IDA-alginate.

distinct stages. One in the range of 30–190 with a maximum decomposition rate at 104°C assigned to the elimination of water adsorbed to the hydrophilic polymer. The other in the range of 210°C–310°C with a maximum decomposition

rate at 248°C ascribed to a complex process including dehydration of the saccharide rings, depolymerization with the formation of water, CO₂ and CH₄ [61]. IDA-functionalized alginate beads show different behaviour. The loss adsorbed water percentage in the first step was reduced and the start of the second stage was gradually shifted to a lower temperature to reach around 165°C. From the thermal gravimetric analysis curves, it can be concluded that the thermal stability of the alginate decreases with the grafting of IDA molecules onto the polysaccharide backbone. That may attribute to the low thermal stability of IDA as a result of the decarboxylation reaction observed in the second degradation step. This phenomenon has also been reported by Naguib [62]. He has indicated that thermal stability of the polymer reduced with the grafting of itaconic acid onto sisal fiber. Isiklan et al. [63] have obtained the same results with alginate grafted with itaconic acid. The adsorption of the MB molecules onto IDA-Alg increased the lost water in the first step compared with the IDA-Alg, while the start of the second stage shifted to a temperature between that of the alginate and the IDA-Alg; 175°C. The third degradation step is the same for the three derivatives; Alg, IDA-Alg, and MB-IDA-Alg. The hydrophilicity of the MB molecules affects the behaviour in the first and second degradation steps compared with the IDA-Alg.

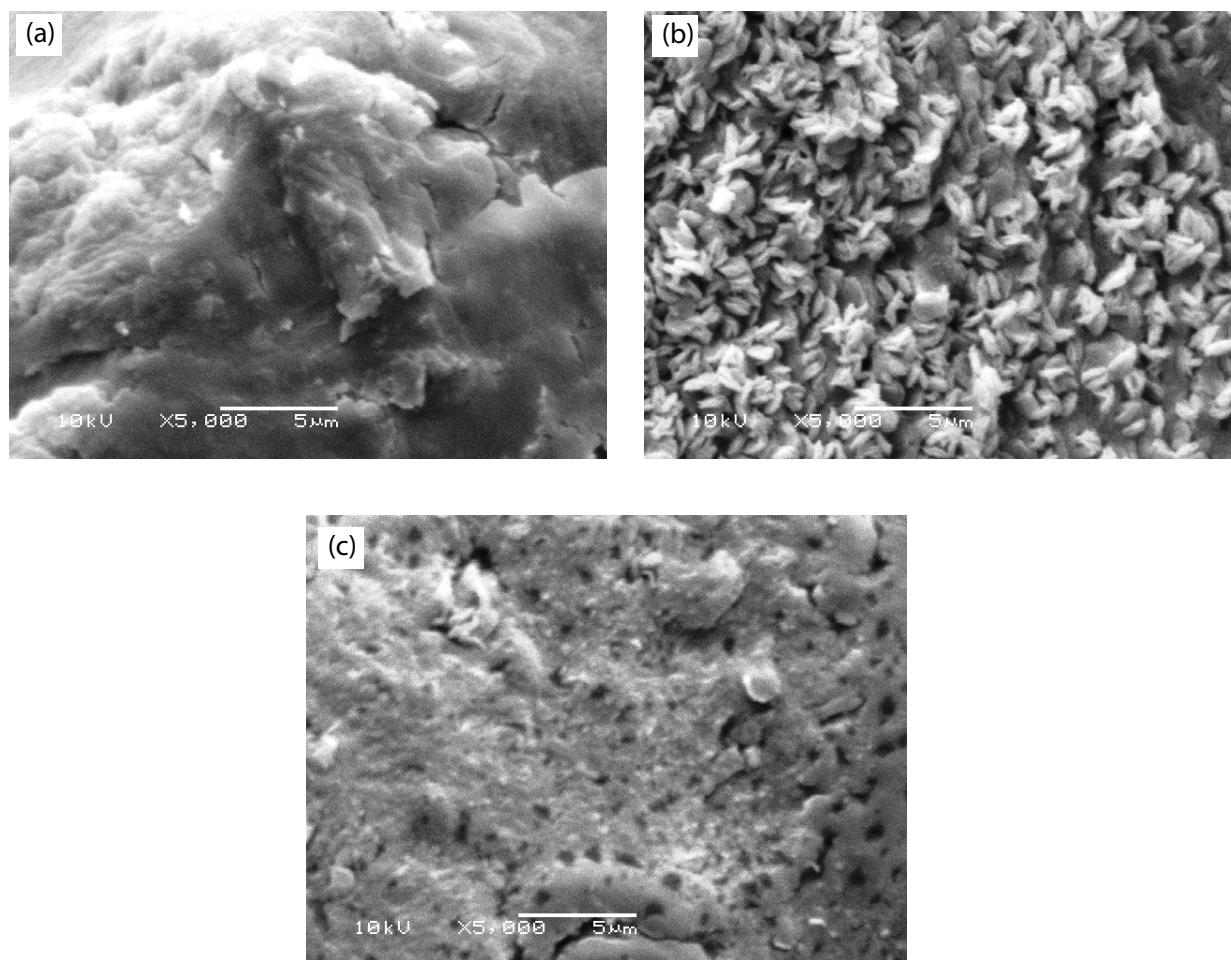


Fig. 10. Scanning electron micrographs of (a) alginate, (b) IDA-alginate, and (c) MB-IDA-alginate.

3.5.3. Scanning electron micrographs

The scanning electron micrographs of alginate, IDA-functionalized alginate, and MB-IDA-functionalized alginate are shown in Fig. 10. By comparing the surface morphology, we found that treatment of the alginate surface with IDA (Fig. 10b) has drastically changed the surface morphology of the alginate (Fig. 10a). As shown in the figure, the surface of the IDA-functionalized alginate has oriented structure (rice-like structure) than that of alginate, which may attribute to the polarity difference between alginate and IDA. At the same time, surface of MB-IDA-functionalized alginate becoming smoother along with the adsorption of the MB molecules (Fig. 10c).

4. Conclusion

CAB for methylene blue (MB) removal have been developed. The alginate concentration variation has a positive effect on both the MB removal percentage and the adsorption capacity. Maximum MB removal percentage and the adsorption capacity were obtained using calcium chloride 2% (W/V) concentration. No significant effect of the crosslinking temperature has been noticed within 30°C–50°C range. Ten min of crosslinking was found to be optimum. Beads size has a small impact. Successive increment of the adsorption capacity has been seen with an increase of MB up to 50 mg/L where fast equilibrium was established within 30 min. The adsorption capacity and the removal percentage are inversely and directly proportional to the variation of the adsorbent amount, respectively. The adsorption process was found to follow the second-pseudo-order kinetics, and the adsorption process followed the Temkin isotherm model. The maximum adsorption capacity at equilibrium was found to be ≈ 14 mg/g.

The impact of drying the beads to a different degree on the adsorbent parameters has been studied to evaluate the practicality of the developed adsorbent. Drying of the beads for 24 h eliminated the contribution of the pore diffusion in the adsorption process. However, the adsorption parameters reduced by about 40%. On the other hand, drying the beads for 5 h improved the adsorption parameters by about 12%. Indeed, the MB diffusion was controlled by both external and internal diffusion mechanism. Furthermore, the type of water found to have neglectable effect on the adsorption process.

References

- [1] G. Sharma, M. Naushad, A. Kumar, S. Rana, S. Sharma, A. Bhatnagar, F.J. Stadler, A.A. Ghfar, M.R. Khan, Efficient removal of coomassie brilliant blue R-250 dye using starch/poly(alginate acid-co-acrylamide) nanohydrogel, *Process Saf. Environ. Protect.*, 109 (2017) 301–310.
- [2] S. Ming-Twanga, M.A.A. Zaini, L.M. Salleh, M.A.C. Yunus, M. Naushad, Potassium hydroxide-treated palm kernel shell sorbents for the efficient removal of methyl violet dye, *Desal. Wat. Treat.*, 84 (2017) 262–270.
- [3] D. Pathania, D. Gupta, A.H. Al-Muhtaseb, G. Sharma, A. Kumar, M. Naushad, T. Ahamad, S.M. Alshehri, Photocatalytic degradation of highly toxic dyes using chitosan-g-poly(acrylamide)/ZnS in presence of solar irradiation, *Photochem. Photobiol. A*, 329 (2016) 61–68.
- [4] D. Pathania, G. Sharma, A. Kumar, M. Naushad, S. Kalia, A. Sharma, Z.A. AlOthman, Combined sorptional–photocatalytic remediation of dyes by polyaniline Zr(IV) selenotungstophosphate nanocomposite, *Toxicol. Environ. Chem.*, 97 (2015) 526–537.
- [5] A. Kumar, G. Sharma, M. Naushad, P. Singh, S. Kalia, Polyacrylamide/Ni_{0.02}Zn_{0.98}O nanocomposite with high solar light photocatalytic activity and efficient adsorption capacity for toxic dye removal, *Ind. Eng. Chem. Res.*, 53 (2014) 15549–15560.
- [6] C.D. Gilson, A.J. Thomas, Encapsulation of lactic acid bacteria with alginate/starch capsules, *Biotechnol. Tech.*, 62 (1997) 227–232.
- [7] S.K. Papageogiou, F.K. Katsaros, E.P. Kouvelos, J.W. Nolan, N.K. Kanellopoulus, Heavy metal sorption by calcium alginate beads from *Laminaria digitata*, *J. Hazard. Mater.*, 173 (2006) 1765–1772.
- [8] J.P. Chen, L. Wang, Calcium alginate based ion-exchange resin and its applications in lead, copper and zinc removal, *Sep. Sci. Technol.*, 36 (2001) 3617–3637.
- [9] S.F. Lim, J.P. Chen, Synthesis of an innovative calcium-alginate magnetic sorbent for removal of multiple contaminants, *Appl. Surf. Sci.*, 253 (2007) 5772–5775.
- [10] J.A. Ramsay, W.H. Mok, Y.S. Luu, M. Savage, Decoloration of textile dyes by alginate-immobilized trametres versicolor, *Chemosphere*, 61 (2005) 956–964.
- [11] T. Aravindhana, N. Fathima, J.R. Rao, B.U. Nair, Equilibrium and thermodynamic studies on the removal of basic black dye using calcium alginate beads, *Colloids Surf. A*, 299 (2007) 232–238.
- [12] M. Kaushal, A. Tiwari, Removal of Rhodamine-B from aqueous solution by adsorption onto crosslinked alginate beads, *J. Dispersion Sci. Technol.*, 31 (2010) 438–441.
- [13] R. Aravindhana, N.N. Fathima, J.R. Rao, B.U. Nair, Utilization of calcium alginate beads as adsorbent for removal of dyes from tannery wastewaters, *JALCA*, 101 (2005) 223–230.
- [14] J.O. Hao, H. Kim, P.C. Chiang, Decolorization of wastewater, *Crit. Rev. Environ. Sci. Technol.*, 30 (2000) 449–505.
- [15] H. Yin, Y. Xia, Y. Li, Effect of Organic Solvents on Dyes Adsorbed by Calcium Alginate, *IOP Conference Series: Materials Science and Engineering*, 382 (2018) 022051.
- [16] V. Rocher, J.-M. Siaugue, V. Cabuil, A. Bee, Removal of organic dyes by magnetic alginate beads, *Water Res.*, 42 (2008) 1290–1298.
- [17] L. Zhu, C. Guan, B. Zhou, Z. Zhang, R. Yang, Y. Tang, J. Yang, Adsorption of dyes onto sodium alginate graft poly(acrylic acid-co-2-acrylamide-2-methyl propane sulfonic acid)/ kaolin hydrogel composites, *Polym. Polym. Compos.*, 25 (2017) 627–634.
- [18] J.M.C. Feira, J.M. Klein, M.M.C. Forte, Ultrasound-assisted synthesis of polyacrylamide-grafted sodium alginate and its application in dye removal, *Polímeros*, 28 (2018) 139–146.
- [19] A. Salisu, M.M. Sanagi, A. Abu Naima, K.J. Karima, Removal of methylene blue dye from aqueous solution using alginate grafted polyacrylonitrile beads, *Der Pharma Chemica*, 7 (2015) 237–242.
- [20] A. Salisu, M.M. Sanagi, K.J. Abd Karim, N. Pourmand, W.A.W. Ibrahim, Adsorption of methylene blue on alginate-grafted-poly (methyl methacrylate), *Jurnal Teknologi (Sci. Eng.)*, 76 (2015) 19–25.
- [21] M.S. Mohy Eldin, E.A. Soliman, A.A. Elzatahry, M.R. Elaassar, M.F. Elkady, A.M. Abdel Rahman, M.E. Yossef, B.Y. Eweida, Preparation and characterization of imino diacetic acid functionalized alginate beads for removal of contaminants from waste water: I. methylene blue cationic dye model, *Desal. Wat. Treat.*, 40 (2012) 15–23.
- [22] S. Li, X. Liu, T. Zou, Removal of cationic dye from aqueous solution by a macroporous hydrophobically modified poly (acrylic acid-acrylamide) hydrogel with enhanced swelling and adsorption properties, *Clean Soil Air Water*, 38 (2010) 378–386.
- [23] S. Langergren, B.K. Svenska, *Veternskapsakad Handlingar, Zur theorie der sogenannten adsorption geloester stoffe*, 24 (1898) 1–39.
- [24] Y.S. Ho, G. McKay, The kinetics of sorption of basic dyes from aqueous solutions by sphagnum moss peat, *Can. J. Chem. Eng.*, 76 (1998) 822–826.

- [25] M. Ozacar, I.A. Sengil, A kinetic study of metal complex dye sorption onto pinedust, *Process Biochem.*, 40 (2005) 565–572.
- [26] Y.S. Ho, G. McKay, Pseudo-second order model for sorption processes, *Process Biochem.*, 34 (1999) 451–465.
- [27] R.L. Tseng, Mesopore control of high surface area NaOH-activated carbon, *J. Colloid Interface Sci.*, 303 (2006) 494–502.
- [28] C. Namasivayam, M.V. Sureshkumar, Removal of chromium (VI) from water and wastewater using surfactant modified coconut coir pith as a biosorbent, *Bioresour. Technol.*, 99 (2008) 2218–2225.
- [29] F.W. Meng, Study on a Mathematical Model in Predicting Breakthrough Curves of Fixed-Bed Removal onto Resin Adsorbent, MS Thesis, Nanjing University, China, 2005, pp. 28–36.
- [30] G. McKay, M.S. Otterburn, J.A. Aja, Fuller's earth and fired clay as adsorbents for dye stuffs, *Water Air Soil Pollut.*, 24 (1985) 307–322.
- [31] W.J. Weber, J.C. Morris, J. Sanity, Kinetics of removal on carbon from solution, *Eng. Div. Am. Soc. Civil Eng.*, 89 (1963) 31–59.
- [32] M. Sarkar, P.K. Acharya, B. Bhaskar, Modeling the removal kinetics of some priority organic pollutants in water from diffusion and activation energy parameters, *J. Colloid Interface Sci.*, 266 (2003) 28–32.
- [33] K. Kannan, M.M. Sundaram, Kinetics and mechanism of removal of methylene blue by removal on various carbons: a comparative study, *Dyes Pigm.*, 51 (2001) 25–40.
- [34] G.E. Boyd, A.W. Adamson, I.S. Myers, The exchange removal of ions from aqueous solutions by organic zeolites; kinetics, *J. Am. Chem. Soc.*, 69 (1947) 2836–2848.
- [35] A.E. Ofomaja, Kinetic study and sorption mechanism of methylene blue and methyl violet onto mansonia (*Mansonia altissima*) wood sawdust, *Chem. Eng. J.*, 143 (2008) 85–95.
- [36] A. Naghash, A. Nezamzadeh-Ejehieh, Comparison of the efficiency of modified clinoptilolite with HDTMA and HDP surfactants for the removal of phosphate in aqueous solutions, *J. Ind. Eng. Chem.*, 31 (2015) 185–191.
- [37] F. Gode, E. Pehlivan, A comparative study of two chelating ion-exchange resins for the removal of chromium(III) from aqueous solution, *J. Hazard. Mater. B*, 100 (2003) 231–243.
- [38] G. Gode, E. Pehlivan, Removal of Cr (III) ions by Turkish brown coals, *Fuel Process Technol.*, 86 (2005) 875–884.
- [39] Y.S. Ho, Effect of pH on lead removal from water using tree fern as the sorbent, *Bioresour. Technol.*, 96 (2005) 1292–1296.
- [40] M.M. Dubinin, E.D. Zaverina, L.V. Radushkevich, Sorption, and structure of activated carbons, I. investigation of organic vapor removal, *Zh. Fiz. Khim.*, 21 (1947) 1351–1362.
- [41] N. Unlu, M. Ersoz, Removal characteristics of heavy metal ions onto a low-cost biopolymeric sorbents from aqueous solution, *J. Hazard. Mater.*, 136 (2006) 272–280.
- [42] A. Mohammad, A.K.R. Rifaqat, A. Rais, A. Jameel, Removal studies on *Citrus reticulata* (fruit peel of orange): removal and recovery of Ni(II) from electroplating wastewater, *J. Hazard. Mater.*, 79 (2000) 117–131.
- [43] Y.S. Ho, J.F. Porter, G. McKay, equilibrium isotherm studies for the sorption of divalent metal ions onto peat: copper, nickel and lead single component systems, *Water Air Soil Pollut.*, 141 (2002) 1–33.
- [44] I.A.W. Tan, A.L. Ahmad, B.H. Hameed, Removal of basic dye using activated carbon prepared from oil palm shell: batch and fixed bed studies, *Desalination*, 225 (2008) 13–28.
- [45] M.S. Mohy Eldin, K.M. Aly, Z.A. Khan, A.E.M. Mekky, T.S. Saleh, A.S. Al-Bogami, Removal of methylene blue from synthetic aqueous solutions with novel phosphoric acid-doped pyrazole-g-poly(glycidyl methacrylate) particles: kinetic and equilibrium studies, *Desal. Wat. Treat.*, 57 (2016) 27243–27258.
- [46] B.H. Hameed, L.H. Chin, S. Rengaraj, Removal of 4-chlorophenol onto activated carbon prepared from rattan sawdust, *Desalination*, 225 (2008) 185–198.
- [47] M.I. Temkin, V. Pyzhev, Kinetics of ammonia synthesis on promoted iron catalysts, *Acta Physicochim.*, 12 (1940) 327–356.
- [48] A. Seker, T. Shahwan, A.E. Eroglu, Y. Sinan, Z. Demirel, M.C. Dalay, Equilibrium, thermodynamic and kinetic studies for the biosorption of aqueous lead(II), cadmium(II) and nickel(II) ions on *Spirulina platensis*, *J. Hazard. Mater.*, 154 (2008) 973–980.
- [49] F. Helfferich, *Ion Exchange*; McGraw-Hill, New York, 1962.
- [50] U.R. Malik, S.M. Hasany, M.S. Subhani, Sorptive potential of sunflower stem for Cr(III) ions from aqueous solutions and its kinetic and thermodynamic profile, *Talanta*, 66 (2005) 166–173.
- [51] J.M. Smith, *Chemical Engineering Kinetics*; McGraw-Hill, New York, 1981.
- [52] Y. Pei, D. Guo, Q. An, Z. Xiao, S. Zhai, B. Zhai, Hydrogels with diffusion-facilitated porous network for improved adsorption performance, *Korean J. Chem. Eng.*, 35 (2018) 2384–2393.
- [53] G. Sharma, M. Naushad, D. Pathania, A. Mittal, G.E. El-desoky, Modification of *Hibiscus cannabinus* fiber by graft copolymerization: application for dye removal, *Desal. Wat. Treat.*, 54 (2015) 3114–3121.
- [54] A.B. Albadarin, M.N. Collins, M. Naushad, S. Shirazian, G. Walker, C. Mangwandi, Activated lignin–chitosan extruded blends for efficient adsorption of methylene blue, *Chem. Eng. J.*, 307 (2017) 264–272.
- [55] E. Daneshvar, A. Vazirzadeh, A. Niazi, M. Kousha, M. Naushad, A. Bhatnagar, Desorption of Methylene blue dye from brown macroalgae: effects of operating parameters, isotherm study and kinetic modeling, *J. Cleaner Prod.*, 152 (2017) 443–453.
- [56] A.A. Alqadami, M. Naushad, Z.A. Allothman, T. Ahamad, Adsorptive performance of MOF nanocomposite for methylene blue and malachite green dyes: kinetics, isotherm and mechanism, *J. Environ. Manage.*, 223 (2018) 29–36.
- [57] G.M. Patel, C.P. Patel, H.C. Trivedi, Ceric-induced grafting of methyl acrylate onto sodium salt of partially carboxymethylated sodium alginate, *Eur. Polym. J.*, 35 (1999) 201–208.
- [58] W. Wei, B. Zhao, M. He, B. Chen, B. Hu, Iminodiacetic acid functionalized magnetic nanoparticles for speciation of Cr(III) and Cr(VI) followed by graphite furnace atomic absorption spectrometry detection, *RSC Adv.*, 7 (2017) 8504–8511.
- [59] M.A. Olivella, N. Fiol, F. de la Torre, J. Poch, I. Villaescusa, A mechanistic approach to methylene blue sorption on two vegetable wastes: cork bark and grape stalks, *Bioresources*, 7 (2012) 3340–3354.
- [60] M. Keilueit, M. Kleber, Molecular-level interactions in soils and sediments: the role of aromatic π -systems, *Environ. Sci. Technol.*, 43 (2009) 3421–3429.
- [61] J. Zhang, Y. Yuan, J. Shen, S. Lin, Synthesis and characterization of chitosan grafted poly (N, N-dimethyl-N-methacryloxyethyl-N-(3-sulfopropyl) ammonium) initiated by ceric (IV) ion, *Eur. Polym. J.*, 39 (2003) 847–850.
- [62] H.F. Naguib, Chemically induced graft copolymerization of itaconic acid onto sisal fibers, *J. Polym. Res.*, 9 (2002) 207–211.
- [63] N. Isiklan, F. Kursun, M. Inal, Graft copolymerization of itaconic acid onto sodium alginate using benzoyl peroxide, *Carbohydr. Polym.*, 79 (2010) 665–672.